Available online at www.sciencedirect.com
ScienceDirect
Journal of Nuclear Materials 367–370 (2007) 610–615
journal of nuclear materials
www.elsevier.com/locate/jnucmat

Brittle–ductile transition in F82H and effects of irradiation

S.J. Noronha *, N.M. Ghoniem

Department of Mechanical and Aerospace Engineering, University of California, Los Angeles, CA 90095-1597, USA

Abstract

We present here a computer simulation model for prediction of the shift in the brittle–ductile transition with irradiation dose. The model is based on discrete dislocation simulation, and is applied to the ferritic/martensitic steel, F82H. The simulated crack system involves microcracks embedded in the plastic zone of a macrocrack. The inherent scatter in fracture toughness measurements are studied by using a size distribution for microcracks, distributed on the crack plane of the macrocrack. The criterion for fracture is the propagation of any of these microcracks located at a distance ahead of the macrocrack. The fracture toughness of F82H at various temperatures is estimated by using measured irradiated and unirradiated yield stress values. Using the yield stress–temperature dependence; the shift in the transition temperature with the irradiation dose is simulated and compared with experiments. Furthermore, the observed scatter in fracture toughness measurements is found to be the result of the distribution in the size of microcracks.

1. Introduction

Predicting the dependence of the ductile–brittle transition temperature (DBTT) on the irradiation dose is important to the safety and reliability of fusion power plants. These steels have microstructure similar to that of ferritic steels widely used in nuclear reactor pressure vessels, and their mechanism of fracture is believed to be similar as in other class of ferritic steels. Odette and He [1] used finite element solutions for crack-tip fields combined with microscopic fracture stress variation with temperature to explain the master curve representation of fracture. Experimental findings [2,3] indicate that the microscopic fracture stress is not sensitive to temperature, and the toughness of F82H depends on temperature and other variables.

Discrete dislocation simulations of crack-tip plasticity have been successful in predicting the brittle–ductile transition (BDT) of simple single crystalline materials (e.g., 4). The advantage of this approach over continuum methods is that fundamental material properties, such as the velocity of dislocations and their interactions are treated explicitly. It was found that the dislocation mobility plays a significant role in determining the transition temperature [4]. However, the variation of the dislocation mobility with temperature alone cannot explain the BDT behavior of microstructurally complex materials, like steels [5]. Recently, we introduced a discrete dislocation simulation model in which the effects of crack-tip blunting are incorporated by using elastic stress fields of blunted cracks [6]. Here, we extend our model to the case where

* Corresponding author.

0022-3115/$ - see front matter
doi:10.1016/j.jnucmat.2007.03.102

microcracks of varying sizes are distributed on (and near) the crack plane.

2. Model and method of calculation

2.1. Problem formulation

It is experimentally established that: (a) the measured microscopic fracture stress (at microcracks) is several orders of magnitude higher than that of the pure Griffith value [2,3] (b) several cracked brittle particles are generally present in the fractured specimens [2,7]; (c) pre-cracks (macrocracks) blunt substantially before the fracture of the specimen occurs in the transition region [8]; (d) the size of carbide precipitates in the matrix has a Poisson distribution [14]. Based on these experimental observations, the present model has the following features.

(1) We consider the emission of dislocations and subsequent shielding from the microcrack-tip. (2) A distribution of microcracks is placed on (and near) the plane of a macrocrack. (3) The failure criterion is that cleavage crack propagation from any of these microcracks near the main crack represents failure. (4) Blunting of the macrocrack is accounted for by modifying the crack-tip field. (5) The size distribution of microcracks is assumed to follow a Poisson distribution; based on the observed fact that carbides sizes has a Poisson distribution and most of them crack early in the loading cycle by due to the plastic deformation of the matrix.

2.2. Overview of the calculation method

A schematic of the model is shown in Fig. 1. On loading, a semi-infinite crack (macrocrack) with microcracks ahead of it on its crack plane emits dislocations from sources near the crack-tip. The arrays of emitted dislocations form the plastic zone of the crack. The macrocrack may also blunt due to dislocation emission. The plastic zone developed at the macrocrack modifies the field ahead of it to that of an elastic–plastic material with hardening [9]. The microcracks placed in this field experience a tensile stress and are assumed to propagate, leading to fracture when the tensile stress on these particles reach a critical value σ_F. During loading, dislocations are emitted from source positions when the resolved shear stress reaches a value $2\tau_y$, where τ_y is the friction stress experienced by dislocations and is due to the effect of all types of obstacles on dislocation motion. The resolved shear stresses are obtained using expressions for a finite crack [10] and a semi-infinite crack [11] for the microcracks and macrocrack, respectively. Emitted dislocations move with a velocity based on the following expression:
when

$$|\tau_{x_i}| > \tau_y, \quad v_{x_i} = \left(\frac{\tau_{x_i} - \tau_y}{\tau_{x_i}}\right)(|\tau_{x_i}|)^m A e^{(-E_a/kT)} \quad \text{and}$$
$$\text{for } |\tau_{x_i}| < \tau_y, \quad v = 0.$$

Parameter values were obtained by fitting the data of screw dislocation motion in iron [12]. The value of m has a linear dependence on temperature, T, $m = 400/T + 1.2$, T is in K, $A = 3.14 \times 10^{-4}$ m s^{-1}(MPa)$^{-m}$ and $E_a = 0.316$ eV. The parameter values corresponding to screw dislocations in elemental iron used should be acceptable, since the movements of dislocations are controlled by the friction stress rather than the velocity it acquires. When the dislocations are in equilibrium the role of dislocation velocity is to move them to there equilibrium position for a given load and dislocation distribution. When dislocations are in their equilibrium positions, the temperature and strain-rate dependence of measured fracture toughness (K_F), plastic zone size (d_F), crack-tip opening displacement, etc. are determined only by the temperature and strain-rate dependence of the friction stress (τ_y). The applied load is incremented at a rate dK/dt (=0.01 MPa $\sqrt{\text{m}}$ s^{-1}); a variable time step is used to make sure dislocations move as an array and numerical instabilities are avoided.

The simulations are performed in two stages: microcracks are first loaded to failure and the obtained microscopic fracture stress (σ_F) values are then used as the fracture criterion in the macrocrack simulations.

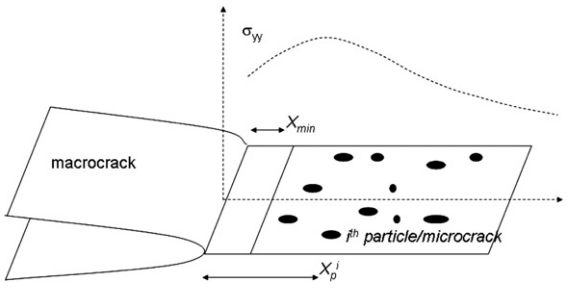

Fig. 1. The geometry of the model used: microcracks (in carbide particles) are distributed in the crack plane ahead of the macrocrack. The propagation of any of the microcracks is the failure criterion in the simulation.

3. Results and discussion

3.1. Microcrack simulation: calculation of microscopic fracture stress (σ_F)

A through-thickness microcrack shown in the inset of Fig. 2 is loaded monotonically, and dislocation sources are allowed to emit dislocations along four symmetric slip planes ($\alpha' = 70°5'$) around the crack. To mimic the triaxial stress field surrounding the microcrack embedded in the plastic zone of a macrocrack, we modified the expressions for the stress fields given in [10] by substituting the applied normal stress with the yield stress. Dislocations are emitted from source positions (here chosen as $4b$, $b = 2.54$ Å); following an earlier study on the effect of source position [9] along the slip planes. The stress fields of emitted dislocations shield the crack-tip from external load. Once moved to their equilibrium positions, the amount of shielding from each dislocation is calculated using expressions from [10] and the total shielding at the crack-tip is obtained by summation. The crack-tip stress intensity is calculated at each time step and when it reaches a pre-assigned critical value $k = K_{Ic} = 1.0$ MPa $\sqrt{m}$ (the Griffith value estimated for Fe with surface energy of 2 J m^{-2}), the crack is assumed to propagate and the corresponding applied load is the microscopic fracture stress (σ_F).

The microscopic fracture stress (σ_F) is estimated for a range of crack sizes from 0.1 to 5 μm. Fig. 2 shows σ_F as a function of the inverse square root of crack size (a), it should be noted that the relation is linear for small crack sizes but deviates for large cracks indicating the greater influence of emitted dislocations. The σ_F is estimated for different friction stresses as well. It should be noted that the fracture stress (σ_F) values of any given crack size overlay one another, and thus (σ_F) is practically independent of temperature consistent with many of the experiments (e.g. [2]). From the best fit curve we interpolate the value of σ_F for a given crack size and friction stress. The value of σ_F thus obtained is used to calculate the macroscopic fracture toughness (K_F).

3.2. Generation of microcrack distribution

To mimic the Poisson distribution [14] of microcracks on the crack plane (mainly originating from the carbides) we generated microcracks with a Poisson distribution of mean radius of 0.5 μm; and uniformly distributed in a 50×50 μm square region. The density of microcracks is taken to be 0.06/μm^2, comparable with the microstructure of typical steels. A typical size distribution of microcracks is shown in Fig. 3. The fracture stress values corresponding to each of these microcracks are estimated from the interpolation of microscopic fracture stress data (in Fig. 2) and are used as input in the next stage of simulation.

3.3. Macrocrack simulation: calculation of fracture toughness (K_F)

The macrocrack is assumed to be semi-infinite, with dislocation sources close to the crack-tip. Dislocations are emitted simultaneously along the two slip planes, symmetrically oriented to the crack plane and inclined at 70.5° to the crack plane. The

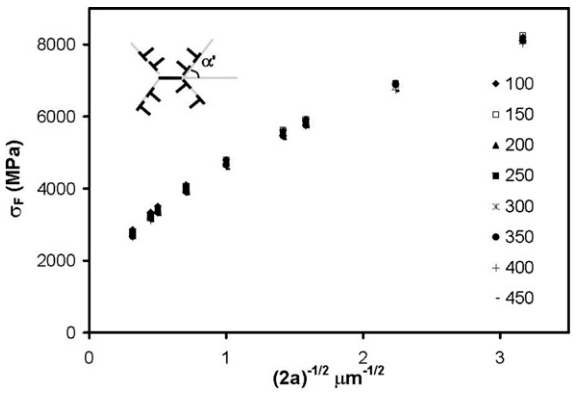

Fig. 2. The microscopic fracture stresses (σ_F) as a function of crack size (a), the values of σ_F is shown for different friction stresses (their values in MPa are shown as labels); in the inset is the geometry of crack-dislocation configuration).

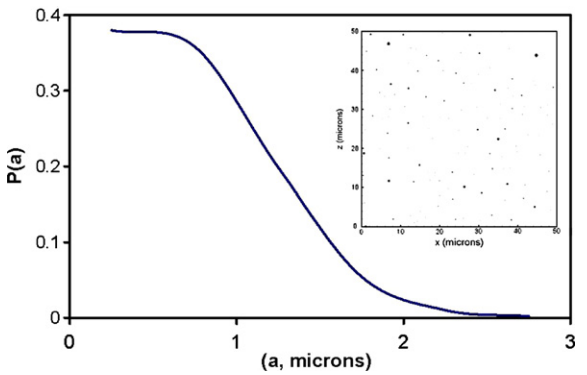

Fig. 3. The distribution of sizes of the microcracks is shown; a Poisson distribution with mean radius of 0.5 μm is used. A plot of distribution of microcracks uniformly distributed in the crack-plane is shown in the inset.

initial source position (x_0) along the slip plane is chosen to be $4b$, where b is the magnitude of Burgers vector. As the load is increased, dislocations are emitted and the crack-tip is blunted. The radius of the blunted crack ρ is taken to be equal to $Nb\sin\alpha$, where N is the number of emitted dislocations, and α is the slip plane angle. As blunting increases: (a) the crack tip fields are modified to be that of a blunted crack [13] (b) source positions are chosen to be equal to the crack-tip radius, (i.e. $x_0 = \rho$), (c) the notional crack-tip from which the image stress of dislocations is calculated is moved back to the center of curvature of the blunted crack. The distribution of microcracks obtained in the previous section is placed ahead of the macrocrack on the crack plane beyond a distance $X_{\min} = 10$ μm (i.e. is about a grain diameter). At each time step, the stress ahead of the crack at distances X_p's (the microcracks are assumed to be at these positions) along the crack plane are calculated. The fracture criterion is the tensile stress (σ^p_{yy}) at any of the particles (at distance X^i_p) reaching σ^i_F. The applied load at the macrocrack gives the fracture toughness (K_F).

We used six different distributions of microcracks for each friction stress; here we report the results obtained for friction stress values from 300 to 600 MPa. As shown in Fig. 4(a), when the friction stress is decreased, the applied stress intensity K required for the tensile stress at X^i_p to reach the critical value σ^i_F increases rapidly. Two factors contributing to this exponential increase could be the decrease in the tensile stress at the microcrack due to crack-tip blunting and the increasing effects of the stress field (predominantly compressive) from emitted dislocations. This can be seen in Figs. 4(b) and 4(c) where the number of dislocations emitted (N_F) and plastic zone size (d_F) for each friction stress measured at fracture, K-applied $= K_F$ is shown. The plastic zone size is the distance measured along the slip plane of the farthest dislocation from the crack-tip. This exponential increase in the fracture toughness corresponds to the transition from brittle to ductile behavior.

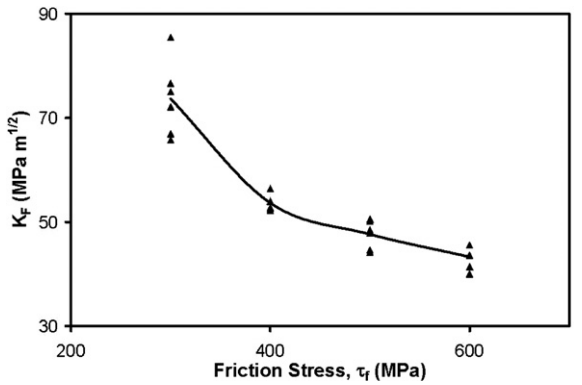

Fig. 4(a). The fracture toughness (K_F) as a function of friction stress for cases with six different microcrack configurations is plotted. The mean value curve is also shown.

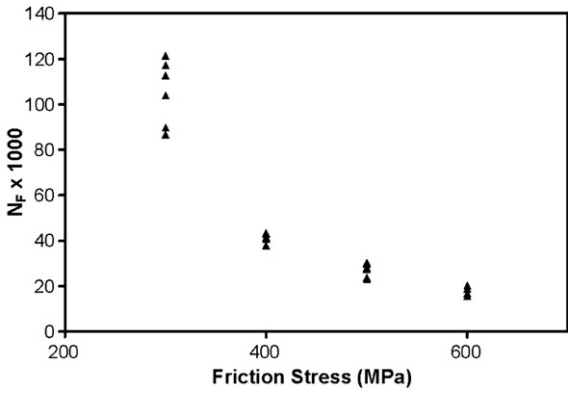

Fig. 4(b). The number of dislocations emitted as a function of friction stress for the six different microcrack configurations.

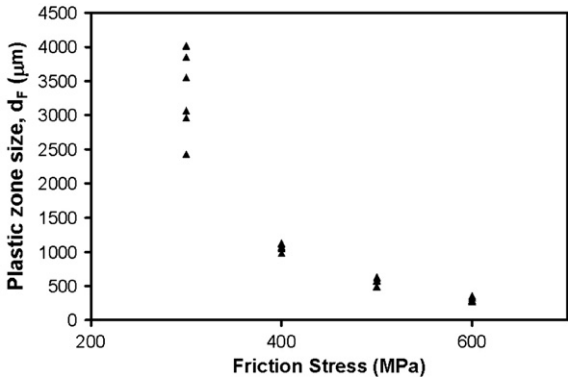

Fig. 4(c). The plastic zone size (d_F) calculated at K_F as a function of friction stress is shown.

Fig. 5(a) shows the scatter of the radius of microcracks that leads to fracture. It should be noted that the size of the microcracks that lead to fracture in all cases are around 2–3 μm and the scatter of these values is very narrow and independent of the friction stress; which is consistent with many experimental findings [2]. On comparing the size of these microcracks with Fig. 3, where a typical size distribution of the crack size is shown, it can be seen that the microcracks that lead to fracture are among the largest in any given sample. However it should be noted from Fig. 5(b), that the distance of these

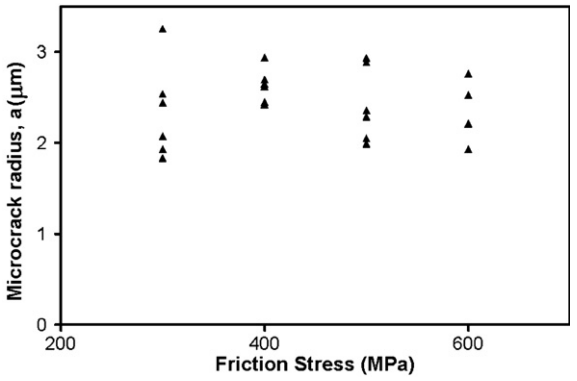

Fig. 5(a). The size of microcracks that lead to fracture for different friction stresses corresponding to Fig. 4(a).

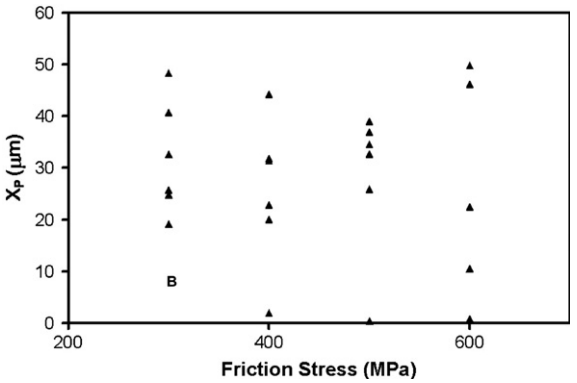

Fig. 5(b). The distance of microcracks that leads to fracture in each simulation reported in Fig. 4(a).

microcracks from the macrocrack-tip varies substantially from case to case and is widely scattered. Even though the X_p is widely scattered, it is found that it is not correlated with the scatter of measured K_F (compare Figs. 4(a) and 5(b)); whereas it appears that the crack size distribution is correlated with K_F (compare Figs. 4(a) and 5(a)) even though their scatter is narrow. This can be further confirmed from Fig. 5(c), where the standard deviations of data in Figs. 4(a), 5(a) and 5(b) are shown. It can be seen that variation of standard deviation of K_F and microcrack radius, a are similar; whereas that of the K_F and X_p are not correlated.

In Fig. 6, the calculated values of fracture toughness are compared with the fracture toughness measurements of unirradiated and irradiated F82H [15]. The friction stress is taken as $\tau_f = \sigma_y/\sqrt{3}$, where σ_y is the experimentally measured uniaxial yield stress. The results from our calculations are shown as closed and open triangles for unirradiated and irradiated cases respectively. It can be seen that

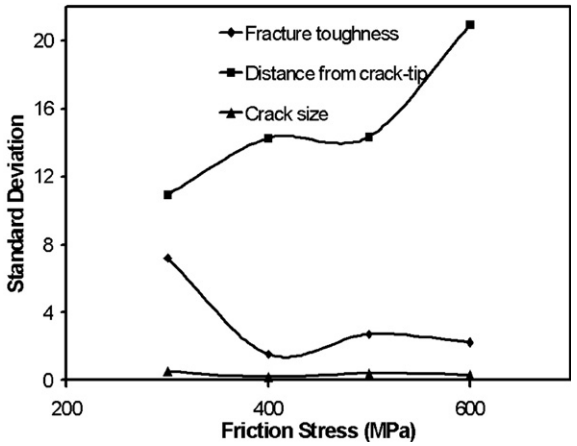

Fig. 5(c). The standard deviations of K_F, a, and X_p values respectively plotted in Figs. 4(a), 5(a) and 5(b).

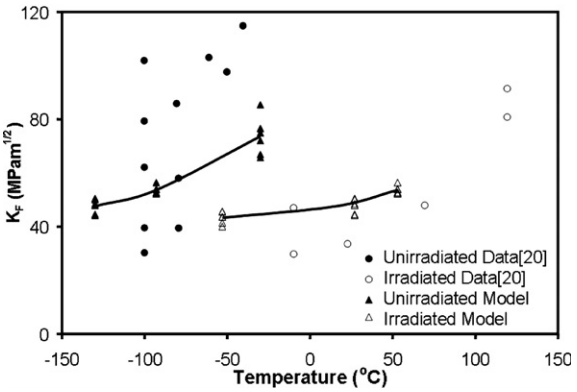

Fig. 6. The fracture toughness values from Fig. 4(a) are plotted as a function of temperature using yield stress–temperature of unirradiated and irradiated F82H. For comparison experimental fracture toughness data from unirradiated and irradiated F82H are also plotted [15]. The closed symbols correspond to unirradiated and open symbols correspond to irradiated data. The mean value curves are shown as continuous lines. The broken lines are guides to show the band of toughness values.

the range of the fracture toughness values, the increase in fracture toughness with temperature, the shift in transition temperature with irradiation and the scatter in K_F values are qualitatively captured with the present model. It should be noted that the shift in the fracture toughness versus temperature curve with the irradiation dose and the more gradual nature of the increase in fracture toughness with irradiation are recovered.

4. Summary and conclusions

We presented a dislocation simulation model to study the ductile–brittle transition in F82H steels.

We find two factors that contribute to the sharp increase in the fracture toughness with temperature are: (a) the increase in the mobility of the emitted dislocations and (b) the effect of crack-tip blunting of the macrocrack. However, usually the experimental measurements of fracture toughness with temperature show wide scatter in values. To address this problem of inherent scatter, we carried out a series of simulations using a distribution of microcracks situated randomly in the crack plane ahead of the macrocrack. On analyzing the statistics of these simulations we found that (a) one among the largest microcracks initiates the fracture in each realization, and (b) the inherent scatter arises from the variation in the size of the microcrack that initiates the fracture and *not* from the variation of its distance from the macrocrack tip. Finally the shift in brittle–ductile transition temperature with irradiation was recovered in the simulation by inputting the corresponding yield stress–temperature data from both irradiated and unirradiated samples.

The two dimensional simulation presented here is an 'approximate' model in the sense we do not account for the complex dislocation mechanisms occur in 3D; like dislocation multiplication processes, which may become significant at higher temperatures near the transition temperature. However, it should be noted that our model still captures the sharp transition at the brittle–ductile transition temperature.

Acknowledgements

Support by US Department of Energy, Office of Fusion Energy, through Grant DE-FG02-03ER54708 is gratefully acknowledged.

References

[1] G.R. Odette, M.Y. He, J. Nucl. Mater 283–287 (2000) 120.
[2] P. Bowen, S.G. Druce, J.F. Knott, Acta Metall. 35 (1987) 1735.
[3] S.R. Ortner, C.A. Hippsley, Mater Sci. Technol. 12 (1996) 1035.
[4] P.B. Hirsch, S.G. Roberts, Philos. Mag. A 64 (1991) 55.
[5] P.B. Hirsch, S.G. Roberts, Philos. Trans. Royal Soc. Lond. A 355 (1997) 355.
[6] S.J. Noronha, N.G. Ghoniem, Metall. Mater. Trans. A 37A (2005) 539.
[7] M.K. Veistinen, V.K. Lindroos, Scripta Metall. 18 (1984) 185.
[8] P. Bowen, J.F. Knott, Metall. Trans. A 17 (1986) 231.
[9] S.G. Roberts, S.J. Noronha, A.J. Wilkinson, P.B. Hirsch, Acta Mater. 50 (2002) 1229.
[10] S. Wang, S. Lee, Mater. Sci. Eng. A 130 (1990) 1.
[11] V. Lakshmanan, J.C.M. Li, Mater. Sci. Eng. A 104 (1988) 95.
[12] H. Saka, K. Nada, T. Imura, Cryst. Latt. Def. 4 (1973) 45.
[13] M. Creager, P.C. Paris, Int. J. Fract. Mech. 3 (1967) 247.
[14] K. Wallin, T. Saario, K. Törrönen, Met. Sci. 18 (1984) 13.
[15] M.A. Sokolov, R.L. Klueh, G.R. Odette, K. Shiba, H. Tanigawa, in: 'Fracture Toughness Characterization of irradiated F82H in the Transition Region', p. 59 in Fusion Materials Semiannual Progress Report, December 31, 2002. DOE/ER-0313/33;<http://www.ms.ornl.gov/programs/fusionmatls/pubs/semiannual.htm>.